Interaction of solitons with extended nonlinear defects

M. T. Primatarowa, K. T. Stoychev, and R. S. Kamburova
Institute of Solid State Physics, Bulgarian Academy of Sciences, 1784 Sofia, Bulgaria
(Received 27 June 2005; published 14 September 2005)

The interaction of nonlinear Schrödinger solitons with extended inhomogeneities with modified nonlinear coefficients is investigated numerically. Decreased nonlinear coefficients act as nonlinear potential steps and yield transmission or reflection of the incoming soliton. For increased nonlinear coefficients (nonlinear potential wells) and a given range of initial velocities and nonlinearity mismatch, the scattering pattern exhibits periodically repeating regions of trapping and transmission as a function of the length of the inhomogeneity. It is shown that the escape of the soliton is due to a resonance between the period of the shape oscillations of the soliton inside the inhomogeneity and the length of the latter. The combined effect of overlapping linear and nonlinear potentials is also investigated.

DOI: 10.1103/PhysRevE.72.036608 PACS number(s): 05.45.Yv

I. INTRODUCTION

The interaction of solitons with defects and inhomogeneities is a problem of considerable theoretical and practical importance. Scattering of nonlinear Schrödinger (NLS) solitons from point defects has been studied in [1–5] and of topological solitons in [6–8]. It has been shown in particular that kinks can be reflected by an attractive impurity via a "two-bounce" resonance mechanism involving the excitation and deexcitation of localized impurity modes [7], or impurity and shape modes [8]. Nonlinear impurity modes in the generalized NLS equation have been studied in detail in [9]. The interaction of NLS solitons with strong localized inhomogeneities in the dispersion or nonlinear coefficients has been studied in [10]. Recent investigations have been devoted to the scattering of solitons from extended inhomogeneities [11–13], and nonclassical behavior has been obtained in [14–18]. Resonant interaction of NLS solitons with wide potential wells has been obtained in [19]. In the present work we study the interaction of solitons with long (compared to the soliton's width) segments with modified nonlinearity. While the interaction with segments with decreased nonlinearity (potential step) is similar to the classical-particle case, the interaction with segments with increased nonlinearity (potential well) exhibits nonclassical behavior, associated with the wavelike character of the solitons. The scattering pattern in this case yields periodically repeating regions of trapping and transmission as a function of the width of the nonlinear potential well.

II. SEGMENTS WITH MODIFIED NONLINEARITY

The NLS equation in the presence of a segment with modified nonlinearity reads

$$i\frac{\partial\alpha}{\partial t}+\frac{\partial^2\alpha}{\partial x^2}+2[1+d(x)]|\alpha|^2\alpha=0,$$

$$d(x)=d \text{ for } x_1\leqslant x\leqslant x_2, \quad d(x)=0 \text{ otherwise}, \qquad (1)$$

where we have assumed the nonlinear coefficient within the segment to be uniform. For $d(x)\equiv 0$, Eq. (1) possesses a fundamental bright soliton solution

$$\alpha(x,t)=\frac{1}{L}\,\mathrm{sech}\,\frac{x-vt}{L}e^{i(vx/2-\omega_0 t)}, \quad \omega_0=\frac{v^2}{4}-\frac{1}{L^2}, \qquad (2)$$

where L and v are the width and velocity of the soliton.

The numerical simulations are based on the discrete version of Eq. (1) which describes the dynamics of nonlinear Bose-type excitations in atomic and molecular chains. The segment is modeled by N equal consecutive defects with modified nonlinear coefficients:

$$i\frac{\partial\alpha_n}{\partial t}+(\alpha_{n+1}+\alpha_{n-1}-2\alpha_n)+2(1+d_n)|\alpha_n|^2\alpha_n=0,$$

$$d_n=d \text{ for } n_1\leqslant n\leqslant n_2, \quad n_2-n_1+1=N, \quad d_n=0 \text{ otherwise}. \qquad (3)$$

For wide solitons compared to the lattice constant ($2L\gg 1$) the discreteness-induced effects are negligible and the solution (2) is stable on ideal lattices (with $d_n\equiv 0$). We checked this numerically for solutions with $L\geqslant 4$ over long-time scales. In the simulations below we used the solution (2) with $L=5.75$ as initial condition, placed 50 sites away from the defect segment to avoid initial radiation decay due to overlapping with the inhomogeneity. A predictor-corrector method [20] was employed, periodic boundary conditions and chains much longer than the defect region. In order to eliminate boundary effects and the spurious interaction of the soliton with emitted radiation revolving along the chain, we introduced a damping term in Eq. (3) near the lattice boundaries. Without the damping term, the norm was conserved to within less than 10^{-6} for the whole course of the simulations, which guarantees the accuracy of the calculations.

The energy of the initial solution (2) when it is far from the defect region is

$$E_s=\int_{-\infty}^{\infty}\left(\left|\frac{\partial\alpha}{\partial x}\right|^2-|\alpha|^4\right)dx=\frac{v^2}{2L}-\frac{2}{3L^3}\equiv E_k-E_{nl}, \qquad (4)$$

where the first term describes the kinetic energy of the free quasiparticles and the second term the nonlinear-interaction energy. The scattering pattern depends in general on the in-

terplay between these two energies and the energy of interaction with the nonlinear defects E_d. Its maximal value, corresponding to a soliton placed in the center of the defect region, is

$$E_d = -d\int_{-N/2}^{N/2} |\alpha|^4 dx = -\frac{2d}{L^3}\tanh\frac{N}{2L}\left(1-\frac{1}{3}\tanh\frac{N}{2L}\right). \tag{5}$$

For inhomogeneities much longer than the soliton extent ($N \gg 2L$),

$$E_d = -\frac{4d}{3L^3}. \tag{6}$$

The effects studied below correspond to the case of "slow solitons" with kinetic energy much smaller than the nonlinear energy $E_k \ll E_{nl}$. This preserves the integrity of the solitons during the scattering. The scattering patterns depend in general on the interplay between E_k and E_d. When $E_k \gg |E_d|$, the solitons are not influenced significantly by the defects, and for $E_k \ll |E_d|$, the solitons can break into reflected and transmitted nonlinear and dispersive waves [1]. In the present work we study the interaction of slow solitons with extended nonlinear inhomogeneities with $E_k \sim |E_d|$, in which case interesting resonance phenomena occur.

For small defect strengths ($|d| \ll 1$) the loss of energy due to emitted radiation at the boundary of the segment is small, and the soliton energy and the norm are nearly conserved. The conservation of energy reads

$$v_0^2 - \frac{4}{3L_0^2} = v^2 - \frac{4}{3L^2}, \tag{7}$$

where v_0, L_0, v, and L are the soliton's velocities and widths in the ideal and defect regions, respectively. The conservation of the norm yields

$$L = L_0/(1+d). \tag{8}$$

Substituting Eq. (8) into Eq. (7) gives the following relation between the velocities in the two regions:

$$v^2 = v_0^2 + \frac{4d(2+d)}{3L_0^2}. \tag{9}$$

The role of the modified nonlinearity on the propagation of the soliton can be evaluated from Eqs. (4) and (8). When it enters a segment with a smaller nonlinear coefficient ($d < 0$) its nonlinear energy decreases and in view of Eqs. (9) and (4) this leads to a decrease of the velocity and kinetic energy of the soliton. Thus a segment with decreased nonlinearity acts on the soliton as a nonlinear potential step. The scattering pattern can be determined from Eq. (9) and depends on the values of v_0, L_0, and d. Real final velocities ($0 < v^2 < v_0^2$) correspond to transmission of the soliton through the potential step, while imaginary values of v ($v^2 < 0$) correspond to exponentially decaying excitation inside the segment. In the latter case the soliton is reflected from the boundary. Figure 1 illustrates the scattering of a soliton with $v_0 = 0.05$ and $L_0 = 5.75$ impinging on a segment with decreased nonlinear coefficients covering 100 lattice sites. The

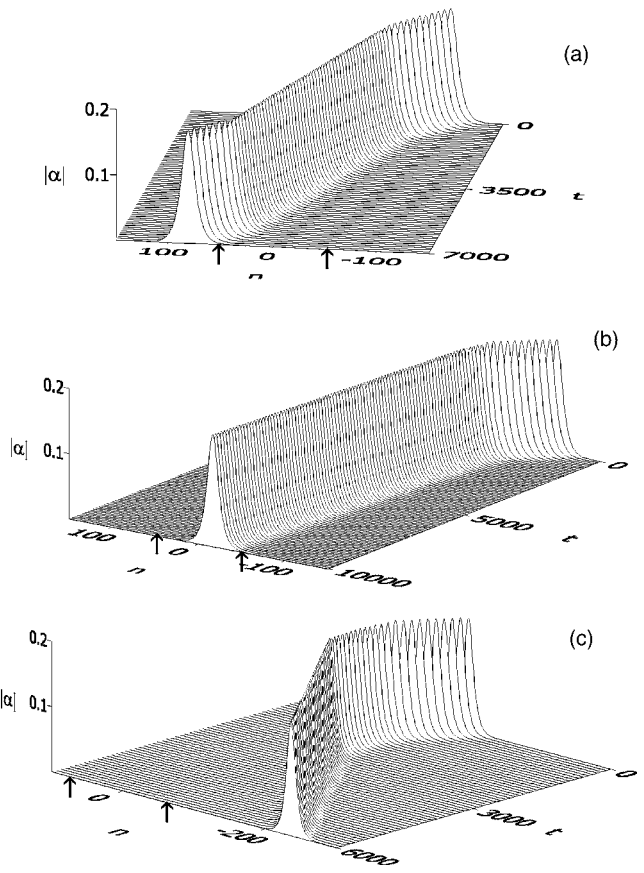

FIG. 1. Transmission and reflection of a soliton from a potential barrier for $v_0 = 0.05$, $L_0 = 5.75$, and $N = 100$. (a) $d = -0.027$ and (b) $d = -0.031$ transmission, (c) $d = -0.032$ reflection. The arrows on the n axis mark the boundaries of the defect region.

simulations show that for $d \geqslant -0.031$ the soliton passes through the segment and escapes to infinity [Figs. 1(a) and 1(b)], while for $d \leqslant -0.032$ it is reflected by the segment [Fig. 1(c)]. This is in excellent agreement with the threshold value $d = -0.0315$ determined from Eq. (9).

The most interesting case, however, is that of a segment with an increased nonlinear coefficient ($d > 0$). This leads to a decrease of the soliton's width (8) and an increase of the nonlinear energy (4) which acts as a nonlinear potential well. The velocity of the soliton inside the segment increases, and in the classical no-damping case the soliton should always pass through such a segment. The numerical simulations, however, showed a different picture: For initial velocities below a lower threshold ($d = 0.2$, $v_0 < 0.038$) the solitons get trapped inside the well and for velocities above an upper threshold ($v_0 > 0.060$) they pass through it and escape to infinity for any segment lengths. For initial velocities in the intermediate region, the scattering pattern as a function of the length of the segment exhibits periodically repeating regions of transmission and capture. This is shown schematically in Fig. 2 where we have plotted the average final velocity of the soliton as a function of the width of the segment for different values of the initial velocity. The lower horizontal parts (with zero final velocity) correspond to trapping of the soliton inside the segment, and the upper horizontal parts with positive final velocity correspond to transmission (the

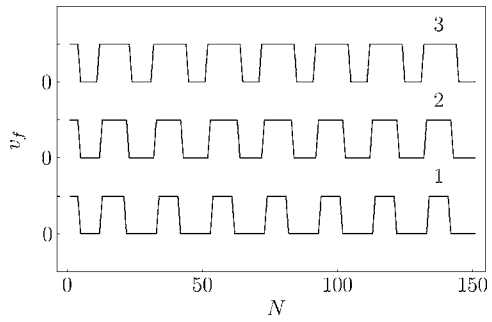

FIG. 2. Periodic regions of capture and transmission as a function of the number N of defects with $d=0.2$ for different initial velocities v_0. The lower horizontal parts (with $v_f=0$) correspond to capture and the upper ones (with $v_f>0$) to transmission. Curves 1, 2, and 3 correspond to $v_0=0.048$, 0.050, and 0.052, respectively.

actual escape velocity varies smoothly in the transmission regions). The increase of the initial velocity (Fig. 2, curves 2 and 3) leads to wider regions of transmission and narrower regions of trapping, while the period of repeat remains nearly constant.

Figure 3 shows the periodic patterns of transmission and capture for fixed initial velocity and two different nonlinear coefficients. As can be expected, the smaller nonlinear coefficient yields wider transmission regions and narrower trapping regions and vice versa, while the total period is nearly unchanged.

Figure 4 illustrates the evolutionary patterns corresponding to transmission and capture. Sharp changes in the soliton velocity mark the boundaries of the inhomogeneity. The velocity of the soliton increases inside the well in accordance with Eq. (9) and drops when it escapes [Fig. 4(a)]. When trapped [Fig. 4(b)], the soliton shuttles inside the well. It is clearly seen that small-amplitude shape oscillations of the soliton are excited at the boundary of the segment and persist for a long time. In order to explain the periodic capture-transmission patterns in Figs. 2 and 3 we looked for a correlation between the period of these oscillations and the length of the segment.

The scattering patterns shown in Fig. 2 have a period of 20 lattice sites. The spatial period of the shape oscillations is not so well defined due to the variable velocity of the soliton inside the segment. The temporal period of the oscillations,

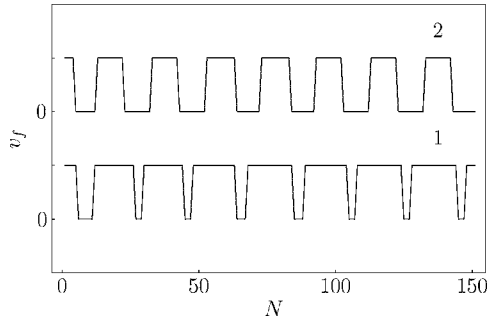

FIG. 3. Periodic regions of capture and transmission as a function of N for $v_0=0.05$ and different depths of the potential well. Curve 1 corresponds to $d=0.18$ and curve 2 to $d=0.20$.

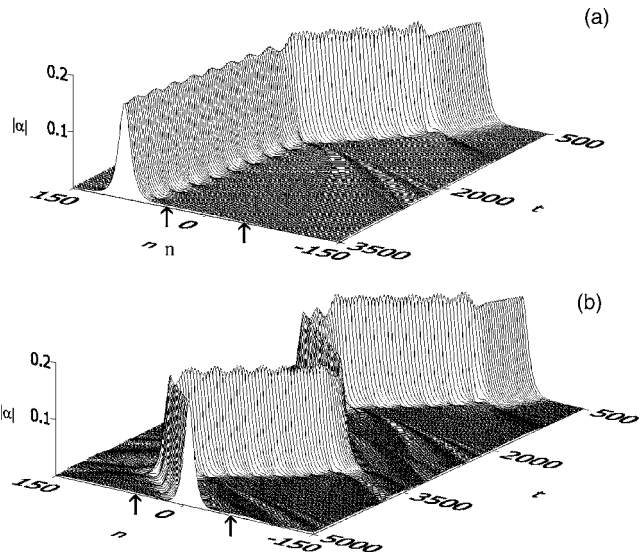

FIG. 4. Evolutionary patterns for (a) transmission ($N=97$) and (b) trapping ($N=107$) for $v_0=0.05$ and $d=0.2$.

however, can be determined with great accuracy from the numerical data. The temporal period inside the inhomogeneity determined from Fig. 4 is $T\approx 140$. It is important to note that this period is measured on top of the soliton maxima—i.e., in a frame moving with the soliton. The corresponding temporal period of the soliton (for $v=0$) inside the defect region is $T=2\pi L_0^2/(1+d)^2=144$ and is in good agreement with the measured one. A theoretical estimate of the spatial period of the oscillations can be obtained from the following considerations: when the soliton enters the nonlinear defect segment, its shape, velocity, and frequency change. The velocities inside the defect region determined from Eq. (9) for $d=0.2$ and initial velocities $v_0=0.048-0.052$ (Fig. 2) are $v=0.142-0.143$. Hence the spatial period of the oscillations is $\Delta x=vT=19.9-20.0$. This is in excellent agreement with the period of the observed capture-transmission patterns in Figs. 2 and 3. The above results show unambiguously that the periodic patterns of trapping and transmission which we observe in the interaction of NLS solitons from extended nonlinear inhomogeneities are due to a resonance between the length of the inhomogeneity and the spatial period of the shape oscillations excited at the boundary or, equivalently, the time for which the soliton crosses the inhomogeneity and temporal period of the shape oscillations.

Shape oscillations of perturbed NLS solitons have been studied by the inverse scattering transform [21–24] as well as by small-amplitude perturbation expansion around the soliton solution [26,27]. Both approaches yield oscillations with frequency $\approx 1/L^2$. Within the second approach, the solution of the perturbed NLS equation can be represented in the form

$$\alpha(x,t)=\{\varphi_0(\xi)+\varphi_1(\xi)e^{-i\omega_1 t}+\varphi_2^*(\xi)e^{i\omega_1 t}\}e^{i(vx/2-\omega_0 t)}, \tag{10}$$

where

$$\varphi_0(\xi) = \frac{1}{L}\,\mathrm{sech}\,\frac{\xi}{L}, \quad \xi = x - vt,$$

is the solution of the unperturbed NLS equation and the functions $\varphi_1(\xi)$ and $\varphi_2(\xi)$ describe the small-amplitude internal modes of the perturbed solution. They satisfy the linear system of equations

$$\frac{\partial^2\varphi_1}{\partial x^2} + \left(4\varphi_0^2 - \frac{1}{L^2} + \omega_1\right)\varphi_1 + 2\varphi_0^2\varphi_2 = 0,$$

$$\frac{\partial^2\varphi_2}{\partial x^2} + \left(4\varphi_0^2 - \frac{1}{L^2} - \omega_1\right)\varphi_2 + 2\varphi_0^2\varphi_1 = 0. \tag{11}$$

The spectrum of Eqs. (11) consists of a discrete eigenvalue $\omega_1 = 0$ corresponding to a static perturbation of the soliton and a band of continuous modes with frequency $\omega_1 = (1/L^2 + \kappa^2)$ [26,27]. The shape oscillations in Fig. 4 have a period $T = 140$ and a frequency $2\pi/T = 0.045$, corresponding to the band-edge frequency of the continuous modes inside the segment ($\omega_1 = 1/L^2 = 0.044$, $\kappa = 0$). The band-edge modes are locked to the soliton, and the corresponding solutions are

$$\varphi_1(\xi) = a_0\left(1 - \mathrm{sech}^2\frac{\xi}{L}\right), \quad \varphi_2(\xi) = -a_0\,\mathrm{sech}^2\,\frac{\xi}{L}, \tag{12}$$

where $a_0 \ll 1/L$.

The periodic scattering patterns in Figs. 2 and 3 can be explained qualitatively in the following way: when the soliton reaches the nonlinear potential it interacts inelastically with the boundary and loses part of its kinetic energy exciting small-amplitude internal modes. The interference of these modes with the soliton yields the observed shape oscillations (or breathing) of the soliton. When the oscillating soliton reaches the second boundary, and different outcomes are possible depending on the timing. In the nonresonant case, the reduced kinetic energy of the soliton is not sufficient to overcome the potential barrier represented by the second boundary, and the soliton is reflected from it and eventually gets trapped. However, the interaction of the oscillating soliton with the boundary is phase sensitive, and if the time for which it crosses the potential well is commensurate with the period of the shape oscillations, the inelastic interaction with the second boundary may extinguish the shape oscillations, transferring their energy back into kinetic energy of the translational motion and allowing the soliton to overcome the barrier and escape to infinity which results in transmission. The higher the initial velocity of the soliton, the wider the transmission regions as seen from Fig. 2.

The escape mechanism described above is not obvious from the three-dimensional plots in Fig. 4(a), as the shape oscillations persist outside the inhomogeneity too. However, a closer inspection of the period of these oscillations reveals a period of $T = 207$, which corresponds to the soliton frequency in the ideal part of the lattice (ω_0 with $v = 0$). Thus the interaction of the oscillating soliton with the second boundary is a complex (two-step) process: the shape oscillations with period $T = 140$ are extinguished which allows the soliton to leaves the inhomogeneity and new shape oscillations with $T = 207$ are excited immediately.

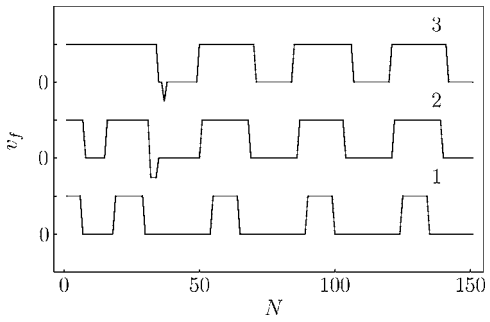

FIG. 5. Capture-transmission-reflection patterns as a function of N for overlapping linear and nonlinear potential wells $v_0 = 0.05$ and $\varepsilon = 0.007$. Curves 1, 2, and 3 correspond to $d = 0.02$, 0.0, and -0.01, respectively.

An increase of the depth of the potential leads to wider regions of trapping and narrower regions of transmission (Fig. 3, curve 2). The perturbation which the boundary induces is stronger in this case, and a larger portion of the kinetic energy of the soliton is transformed into shape modes. Hence a more exact resonance condition is required at the second boundary for the escape of the soliton, which yields narrower regions of transmission. The period of the scattering patterns in this case determined from Fig. 2 is 38 lattice sites, while the spatial period of the corresponding shape oscillations deduced from Eq. (9) is 38.6. Again we witness an excellent agreement between the two.

III. SEGMENTS WITH MODIFIED LINEAR AND NONLINEAR COEFFICIENTS

In [19] we investigated similar resonant transmission effects in the interaction of solitons with wide potential wells represented by a rectangular linear potential. It corresponds to a segment with a decreased energy of the linear excitations forming the soliton or, equivalently, to a decreased phase velocity of the soliton's carrier wave. It is interesting to evaluate the combined effect of overlapping external linear and nonlinear potentials. The NLS equation in the case of overlapping inhomogeneities in the linear and nonlinear terms reads

$$i\frac{\partial\alpha_n}{\partial t} + \varepsilon_n\alpha_n + (\alpha_{n+1} + \alpha_{n-1} - 2\alpha_n) + 2(1 + d_n)|\alpha_n|^2\alpha_n = 0,$$

$$\varepsilon_n = \varepsilon, \quad d_n = d \text{ for } n_1 \leqslant n \leqslant n_2, \quad n_2 - n_1 + 1 = N,$$

$$\varepsilon_n = d_n = 0 \text{ otherwise}. \tag{13}$$

Depending on the signs of ε and d, the two inhomogeneous terms can have additive or compensatory action. The positive signs correspond overlapping linear and nonlinear potential wells, and the combined effect is illustrated in Fig. 5, curve 1. As can be expected, the so-formed deeper potential well yields wider regions of trapping and narrower regions of transmission. When ε and d have opposite signs, the perturbing potential is a combination of a linear potential well and a nonlinear potential well or vice versa. The evolu-

tionary pattern for this case is shown in Fig. 5, curve 3, and corresponds to a shallower potential well. It is worth noting that a complete compensation in this case is not possible due to the different shapes of the potentials.

In some rare cases the resonant condition for escape is achieved after the soliton has crossed the defect region twice in the forward and backward directions. This yields the observed narrow dips in Fig. 5, curves 2 and 3, corresponding to $v_f<0$. They are analogous to the three-bounce resonances observed in [25]. Due to the radiation losses at each boundary, these higher-order resonances are very sharp, extremely sensitive to the initial velocity, and difficult to observe.

IV. CONCLUSION

In summary, we have studied numerically the interaction of slow NLS solitons with extended inhomogeneities in the nonlinear coefficient with variable widths. For the case of increased nonlinear coefficients and initial velocities within a given range, we have obtained periodically repeating regions of trapping and transmission as a function of the width of the inhomogeneity. The observed scattering patterns are explained by an excitation and a following resonant deexcitation of shape oscillations of the solitons at the boundaries of the well. The analysis of these oscillations shows that they are due to excitation of internal modes with frequency from the band edge of the continuous spectrum. In the nonresonant case, due to loss of kinetic energy, the solitons get trapped inside the well. Whenever the time for which the solitons cross the well is commensurate with the period of the shape oscillations, the interaction with the second boundary may extinguish the shape modes, adding their energy back to the kinetic energy of the solitons and allowing the latter to escape to infinity (transmission). The combined effect of overlapping linear and nonlinear inhomogeneities yields additive or compensatory action depending on the signs of the coefficients.

ACKNOWLEDGMENT

This work is supported in part by the National Science Foundation of Bulgaria under Grant No. F1414.

[1] Yu. S. Kivshar, A. M. Kosevich, and O. A. Chubykalo, Zh. Eksp. Teor. Fiz. **93**, 968 (1987) [Sov. Phys. JETP **66**, 545 (1987)].
[2] Yu. S. Kivshar, A. M. Kosevich, and O. A. Chubykalo, Phys. Lett. A **125**, 35 (1987).
[3] D. I. Pushkarov and R. D. Atanasov, Phys. Lett. A **149**, 287 (1990).
[4] X. D. Cao and B. A. Malomed, Phys. Lett. A **206**, 177 (1995).
[5] V. V. Konotop, D. Cai, M. Salerno, A. R. Bishop, and N. Grønbech-Jensen, Phys. Rev. E **53**, 6476 (1996).
[6] Yu. S. Kivshar, Zhang Fei, and L. Vázquez, Phys. Rev. Lett. **67**, 1177 (1991).
[7] Zhang Fei, Yu. S. Kivshar, and L. Vázquez, Phys. Rev. A **45**, 6019 (1992).
[8] Zhang Fei, Yu. S. Kivshar, and L. Vázquez, Phys. Rev. A **46**, 5214 (1992).
[9] A. A. Sukhorukov, Y. S. Kivshar, O. Bang, J. J. Rasmussen, and P. I. Christiansen, Phys. Rev. E **63**, 036601 (2001).
[10] S. Burtsev, D. J. Kaup, and B. A. Malomed, Phys. Rev. E **52**, 4474 (1995).
[11] R. Scharf and A. R. Bishop, Phys. Rev. A **46**, R2973 (1992).
[12] J. J.-L. Ting and M. Peyrard, Phys. Rev. E **53**, 1011 (1996).
[13] H. Frauenkron and P. Grassberger, Phys. Rev. E **53**, 2823 (1996).
[14] G. Kälbermann, Phys. Rev. E **55**, R6360 (1997).
[15] G. Kälbermann, Phys. Lett. A **252**, 37 (1999).
[16] G. Kälbermann, Chaos, Solitons Fractals **12**, 2381 (2001).
[17] G. Kälbermann, Chaos, Solitons Fractals **12**, 625 (2001).
[18] Y. Nogami and F. M. Toyama, Phys. Lett. A **184**, 245 (1994).
[19] K. T. Stoychev, M. T. Primatarowa, and R. S. Kamburova, Phys. Rev. E **70**, 066622 (2004).
[20] L. F. Shampine and M. K. Gordon, *Computer Solution of Ordinary Differential Equations* (Freeman, San Francisco, 1975).
[21] J. Satsima and N. Yajima, Suppl. Prog. Theor. Phys. **55**, 284 (1974).
[22] J. P. Gordon, J. Opt. Soc. Am. B **9**, 91 (1992).
[23] M. W. Chbat, J. P. Prucnal, M. N. Islam, C. E. Soccolich, and J. P. Gordon, J. Opt. Soc. Am. B **10**, 1386 (1993).
[24] E. A. Kuznetsov, A. V. Mikhailov, and I. A. Shimokhin, Physica D **87**, 201 (1995).
[25] D. K. Campbell and M. Peyrard, Physica D **18**, 47 (1986).
[26] Yu. S. Kivshar, D. E. Pelinovsky, T. Cretegny, and M. Peyrard, Phys. Rev. Lett. **80**, 5032 (1998).
[27] D. J. Kaup, Phys. Rev. A **42**, 5689 (1990).